Static Magnetic Field

Wenjie Qiu [1], Jian Zhang [2], Yongkang Luo [2], and Xiaotao Han [2]

[1]Wuhan National High Magnetic Field Center
[2]Affiliation not available

October 30, 2023

Abstract

Ultrasonic measurements at high magnetic field and low temperature necessitate ultra-fast excitations, ultra-high dynamic range of duty-cycle adjustments, as well as real-time, precise and automatic analysis. This paper proposes a dual-mode ultrasonic measurement system, which means the capability of carrying out acoustic measurements in both pulsed and static high magnetic field with low temperature. Based on the "counter-delay-chain" series structure and adaptive jitter compensation in the field-programmable-gate-array(FPGA), the timing control accuracy of 5 nanoseconds and the timing jitter below 160 picoseconds are realized for high-resolution excitation generation and precise sampling window adjustment. The duty cycle adjustment achieves a high dynamic range from 0.23 ppb to 10 % to realize both pulsed field mode and static field mode (denoted as PF-mode and SF-mode) ultrasonic measurements. The independent sampling window adjustment reduces the data size by more than 80%, extends the maximum testing duration and reduces the analysis consuming. Combined with the automatic cross-correlation analysis method, this system can automatically carry out PF-mode tests with a repetition rate above 100 kHz and SF-mode tests for hours with sound velocity accuracy of 2%. Experiments have proved the reliability and feasibility of the system and revealed its application prospect in condensed matter physics experiments.

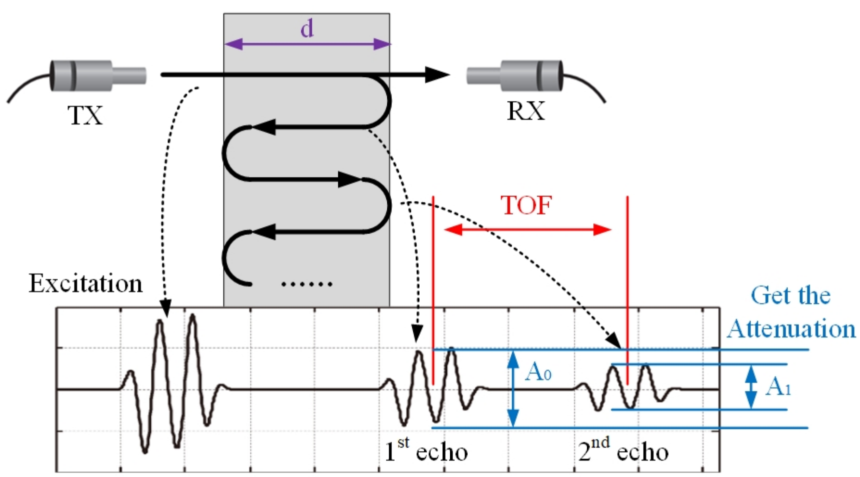

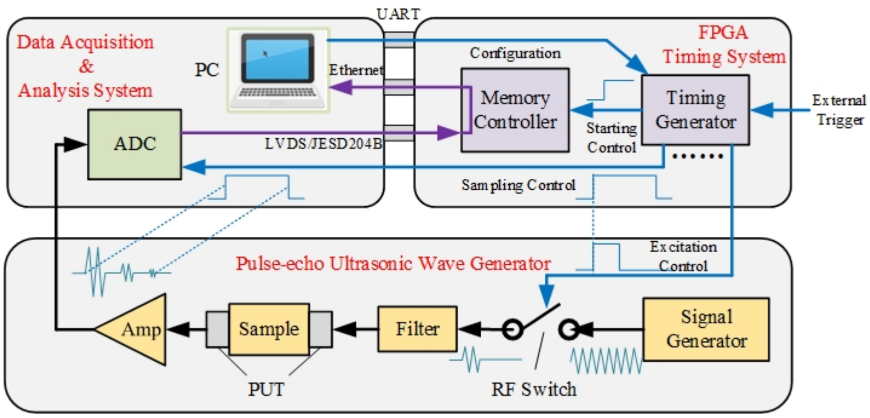
UART
Data Acquisition
&
Analysis System
PC
Ethernet
ADC
LVDS/JESD204B
FPGA
Timing System
Configuration
Memory
Controller
Timing
Generator
External
Trigger
Starting
Control
Sampling Control
Excitation
Control
Pulse-echo Ultrasonic Wave Generator
Amp
Sample
Filter
Signal
Generator
PUT
RF Switch

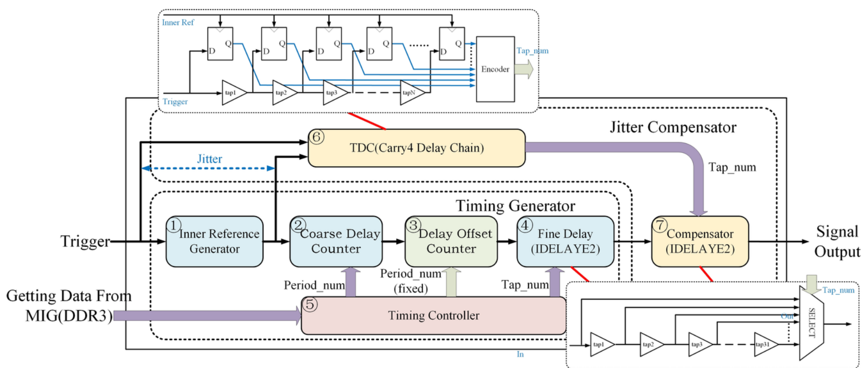
Inner Ref
Trigger
Encoder
Tap_num
Jitter Compensator
TDC(Carry4 Delay Chain)
Jitter
Tap_num
Timing Generator
Trigger
Inner Reference
Generator
Coarse Delay
Counter
Delay Offset
Counter
Fine Delay
(IDELAYE2)
Compensator
(IDELAYE2)
Signal
Output
Period_num
Period_num
(fixed)
Tap_num
Getting Data From
MIG(DDR3)
Timing Controller
SELECT

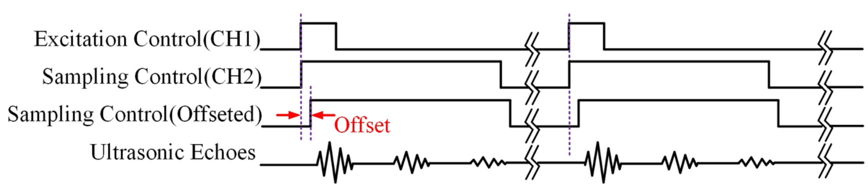
Excitation Control(CH1)
Sampling Control(CH2)
Sampling Control(Offseted)
Offset
Ultrasonic Echoes

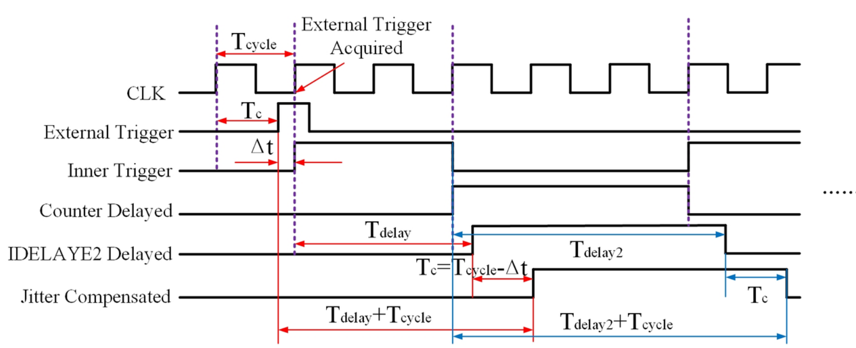
Tcycle
External Trigger
Acquired
CLK
Tc
External Trigger
Δt
Inner Trigger
Counter Delayed
Tdelay
IDELAYE2 Delayed
Tdelay2
Tc=Tcycle-Δt
Jitter Compensated
Tc
Tdelay+Tcycle
Tdelay2+Tcycle
......

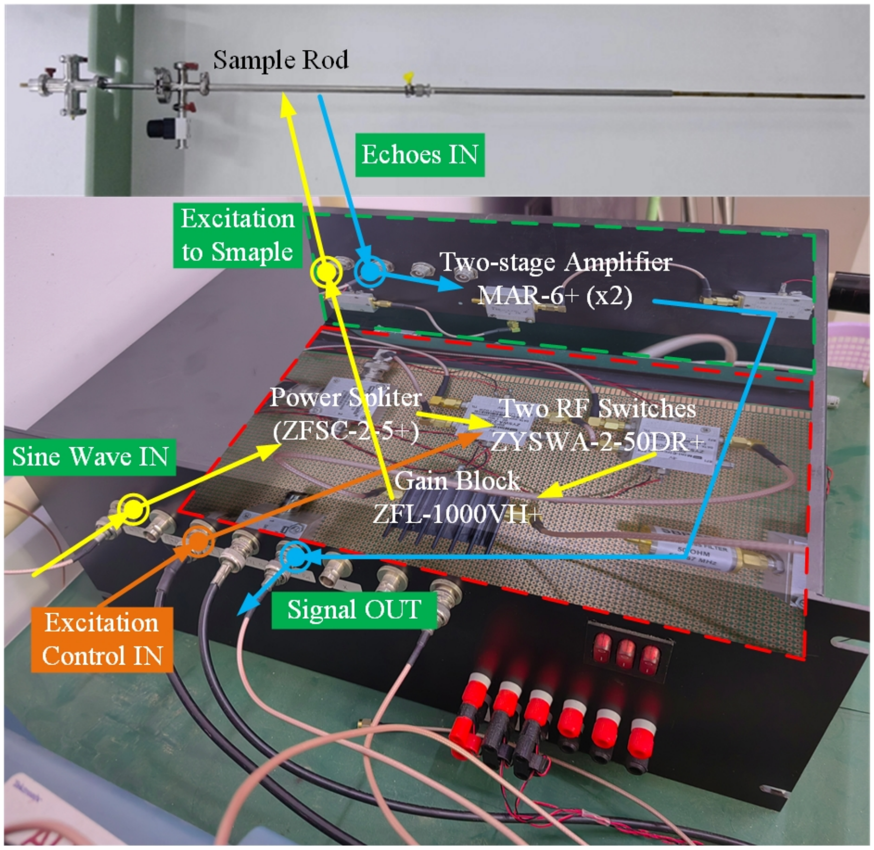
Sample Rod
Echoes IN
Excitation to Smaple
Two-stage Amplifier MAR-6+ (x2)
Power Spliter (ZFSC-2-5+)
Two RF Switches ZYSWA-2-50DR+
Sine Wave IN
Gain Block ZFL-1000VH+
Excitation Control IN
Signal OUT

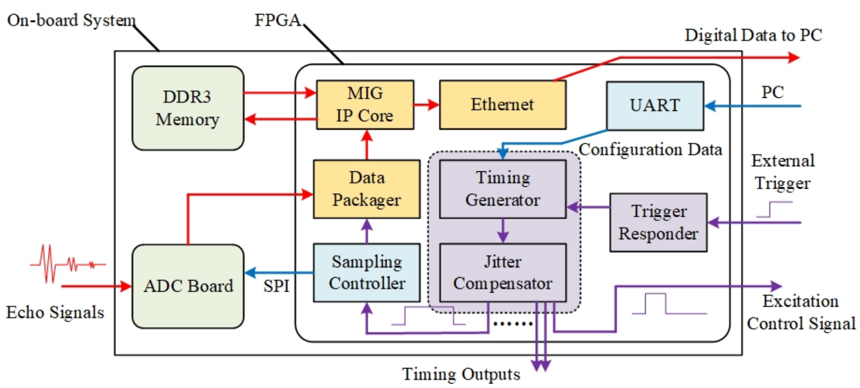
On-board System
FPGA
Digital Data to PC
DDR3 Memory
MIG IP Core
Ethernet
UART
PC
Configuration Data
Data Packager
Timing Generator
External Trigger
Trigger Responder
ADC Board
SPI
Sampling Controller
Jitter Compensator
Echo Signals
Excitation Control Signal
Timing Outputs

figures/Fig8/Fig8-eps-converted-to.pdf

figures/Fig9-a/Fig9-a-eps-converted-to.pdf figures/Fig9-b/Fig9-b-eps-converted-to.pdf

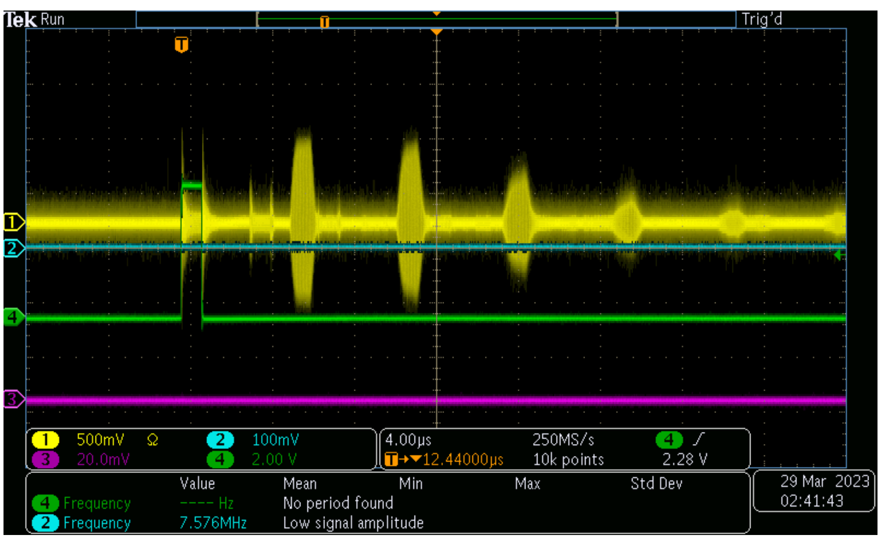

figures/Fig11/Fig11-eps-converted-to.pdf

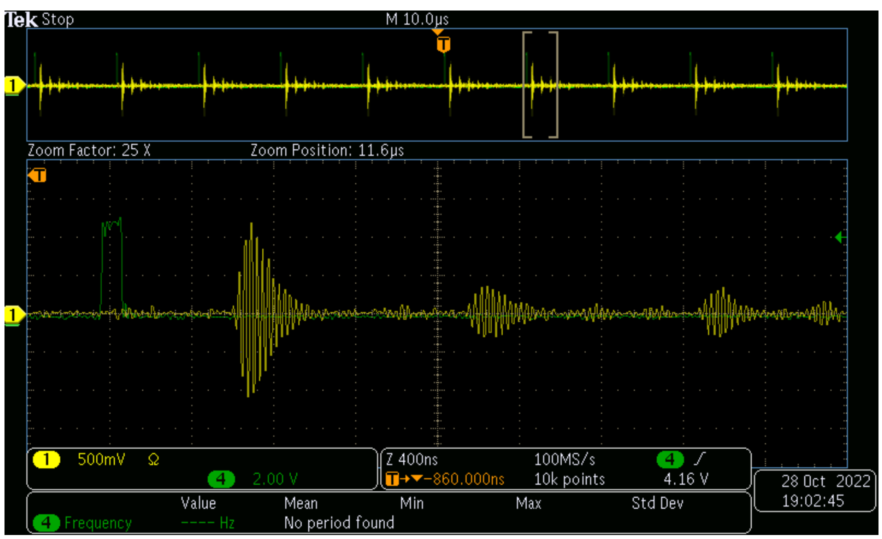

figures/Fig13/Fig13-eps-converted-to.pdf

figures/Fig14/Fig14-eps-converted-to.pdf

An Integrated Dual-mode Pulse-echo Ultrasonic Measurement System Under Pulsed/Static Magnetic Field

Wenjie Qiu, Jian Zhang, Yongkang Luo, and Xiaotao Han, *Senior Member, IEEE*

Abstract*—Ultrasonic measurements at high magnetic field and low temperature necessitate ultra-fast excitations, ultra-high dynamic range of duty-cycle adjustments, as well as real-time, precise and automatic analysis. This paper proposes a dual-mode ultrasonic measurement system, which means the capability of carrying out acoustic measurements in both pulsed and static high magnetic field with low temperature. Based on the "counter-delay-chain" series structure and adaptive jitter compensation in the field-programmable-gate-array(FPGA), the timing control accuracy of 5 nanoseconds and the timing jitter below 160 picoseconds are realized for high-resolution excitation generation and precise sampling window adjustment. The duty cycle adjustment achieves a high dynamic range from 0.23 ppb to 10 % to realize both pulsed field mode and static field mode (denoted as PF-mode and SF-mode) ultrasonic measurements. The independent sampling window adjustment reduces the data size by more than 80%, extends the maximum testing duration and reduces the analysis consuming. Combined with the automatic cross-correlation analysis method, this system can automatically carry out PF-mode tests with a repetition rate above 100 kHz and SF-mode tests for hours with sound velocity accuracy of 2%. Experiments have proved the reliability and feasibility of the system and revealed its application prospect in condensed matter physics experiments.

***Index Terms*—Ultrasonic Measurement; Pulse-echo; High Magnetic Field; Dual-mode; Timing Generator; FPGA**

I. INTRODUCTION

Ultrasonic measurement is an effective means to probe properties of materials. Give pulsed-sinusoidal excitation signals to a transducer to transmit sound waves to the sample, receive the echo sequence from the other side, and the sound velocity and attenuation can be calculated by the time of flight (TOF) and amplitude variation between echoes. In condensed matter physics, acoustic properties of solids such as elastic moduli and Poisson's ratio can be analyzed to characterize their mechanical properties and describe the phase transition or the symmetry of the order parameter. High magnetic field and low temperature has been proved to be an effective way of inducing change of properties [1]. Many significant physical phenomena have been observed by ultrasonic measurement in high magnetic field and low temperature such as the phase transition and quantum oscillation of $CeRhIn_5$ [2],[3] and TaAs [4], the spin-lattice effect by means of measuring the elastic moduli [5],[6],[7] the Kondo effect [8] and the magnetostructural transition [9]. Usually, measurements under both pulsed and static magnetic fields should be carried out for the observation of different positions of the phase transition [3],[8],[9],which corresponds to the requirement of a "PF/SF" dual-mode test system. And the dual-mode method can also be applied in the industrial field for destructive testing [10] or long-term monitoring of hydrogen embrittlement susceptibility [11].

For the growing requirements in microcosmic physics, an ultra-high magnetic field ultrasonic measuring facility is under construction at the Wuhan National High Magnetic Field Center (WHMFC). It provides extreme conditions for ultrasonic experiments on a variety of materials by producing pulsed magnetic fields up to 94.8 T or quasi-static magnetic fields up to 64 T and a constant temperature environment from 1.71 K to 77 K [12]. In order to observe phase transition of samples (like $CeRhIn_5$) in pulsed magnetic field or their acoustic parameter changes caused by other condition changes in static magnetic field, a dual-mode ultrasonic measurement system capable of accurately and automatically monitoring the acoustic properties of materials in different temperatures and magnetic fields (especially in low temperature and high magnetic field environment) is needed. Besides the sound velocity accuracy of at least 2% (an error of about 80 m/s for $CeRhIn_5$) [3], additional requirements are raised for the measurement system in the high magnetic field.

1) The pulse width of the excitation should be narrow enough, such as nanosecond level to reduce the risk of overlapping of two adjacent echoes. In the 55 T magnet in the WHMFC, only samples shorter than 5mm can be inserted, making it necessary to shorten the pulse width less than 1 μs.
2) A large dynamic range of the duty ratio of the excitation (0.23ppb to 2 %, equivalent to the repetition rate of 50mHz ~ 100kHz) should be provided without modifying the hardware facilities, in order to meet the requirement of high-density measurements in PF-mode and long-term observation in SF-mode,
3) Data size needs to be reduced to extend the maximum of

The authors are with the Wuhan National High Magnetic Field Center, Huazhong University of Science and Technology and the State Key Laboratory of Advanced Electromagnetic Engineering and Technology, Huazhong University of Science and Technology, Wuhan 430074, China. Xiaotan Han is the corresponding author (e-mail: xthan@mail.hust.edu.cn).

test duration and reduce the computation. Most of the part of the time-domain echo sequence contains only noise with nothing useful, especially in stable field tests. Find a way to pick up only the useful part of ultrasonic signals can optimize the utilization of memories and test speed.

4) An accurate external trigger module is needed for both PF-mode and SF-mode to generate excitations just at the moment that the magnetic field is generated. And the trigger time should be stable with low-jitter to avoid a large displacement in the v-B curve.

Although traditional function generator or pulse generator can be used to generate the excitation [13],[14], the lack of dynamic range of their duty ratio makes it difficult to meet the requirements of SF-mode (requirements 1 and 2 above). Sampling window control and data size reduction may be realized with the help of the "sequence mode" of the oscilloscope [1]. However, it lacks the ability of adjusting the position of the sampling window precisely in the time-domain referring to the excitation control signal and it's hard to setup an ultra-small duty ratio for SF-mode. Recently, FPGA-based ultrasonic excitation controller has been proposed [15],[16], based on digital-to-time technology and the on-chip clocking tree. Although their timing generator based on FPGA make it possible to meet the requirements 1~3 at the same time, they are short of the function of high-accuracy external trigger mode and is unable to meet the requirement 4.

According to the demands of precision, stability and flexibility of controller, this paper proposes a dual-mode ultrasonic measurement control system, which contains a multi-channel timing system, and a data acquisition & automatic analyzing system. The FPGA based multi-channel ultrasonic timing system is the extension and upgrading of our previous works [17] with a timing resolution of 5 ns/78 ps (for the **Req.1**), a timing range of 5 ns~21.5 s (for the **Req.2**) can be realized, and a timing jitter in external trigger mode within 160 ps (for the **Req.4**). Attached by a configurable offset-chain, it can be much easier to make the position of the sampling window consistent with the positions of ultrasonic echoes and reduce the data size by more than 80%, extending the maximum duration of ultrasonic experiments in pulsed field for 2 seconds or stable field for several hours (for the **Req.3**). Combined with cross-correlation and fast-Fourier-transform (FFT) method, a self-designed timing control and acoustic parameter analyzing software is implemented on LabVIEW to generate the "velocity/attenuation-magnetic field" curve quickly and automatically with sound velocity accuracy of 2%. Compared with other ultrasonic systems, this highly integrated ultrasonic measurement control system has realized dual-mode measurements and automatic analysis with the same velocity accuracy as others and a smaller data size. And the capability of dual-mode ultrasonic testing control has been verified by several tests.

II. Design and Principle

A. Pulse-echo ultrasonic measurement method

The process of pulse-echo ultrasonic measurements with tone-burst excitations is shown in Fig.1. A simple pulse-echo measurement system consists of a TX piezoelectric ultrasonic transducer (PUT), the sample, and a RX PUT.

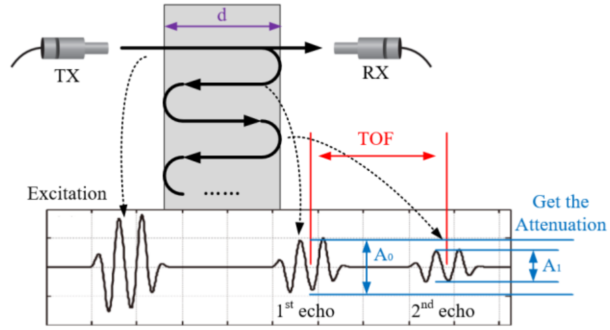

Fig. 1. Principle of the pulse-echo ultrasonic measurements

The TX transducer is excited by pulsed sine waves and generates sound waves with the same shape. Ultrasonic wave transports in the sample and generates multi-reflected echoes, which will be received by the RX transducer on the other side of the sample. According to the TOF between neighboring echoes, the acoustic sound velocity can be calculated. And the acoustic attenuation can be analyzed by the change of the amplitude.

Echo signals should be located in the time domain and be cut out from the echo sequences to be analyzed. The onset of each echo can be recognized automatically based on the multi-threshold method [18] or the Histogram distance method [19], or be artificially observed in a pre-experiment. Once the location of the first few echoes are pinpointed, the echoes under other excitation pulses will be automatically determined if a high-precision and high-stability excitation generating control can be provided.

TOF is calculated by the cross-correlation method, which is widely used [20],[21]. Cut out each echo (y_1 and y_2) and find the location in the time-domain when their cross-correlation factor reached the maximum, then the TOF is:

$$\tau_1 = \arg\max_{\tau} \left\{ \int_{-\infty}^{\infty} y_1(t)\, y_2(t-\tau)\, dt \right\} \tag{1}$$

Give the sample length d, and the sound velocity v can be calculated by: (the sound velocity of longitude mode v_l and shear mode v_s should be tested by independent experiments)

$$v = \frac{2d}{\tau_1} \tag{2}$$

The acoustic attenuation can be recognized as the change of the amplitude of the center frequency component according to FFT results: (A_0 and A_1 represent the amplitude of the first and the second echo, shown in Fig.1)

$$\alpha = \frac{20}{2d} \log \frac{A_0}{A_1} \tag{3}$$

These two results can be considered as instantaneous parameter if the repetition rate of excitation can be high enough. According to the sound velocity and attenuation, many other physical quantities, such as elastic stiffness tensor, bulk/shear elastic modulus, Young's modulus, Poisson's ratio and so on, can be calculated, shown in Table.I (cubic crystal).

TABLE I
CALCULATION FOR TYPICAL PHYSICAL QUANTITIES (CUBIC)

Physical Quantity	Calculation Formula
Elastic stiffness tensor	$c_{11}=\rho\upsilon_l^{\,2}$, $c_{44}=\rho\upsilon_s^{\,2}$, $c_{12}=c_{11}-2c_{44}$
Bulk and Shear elastic modulus	$K=\dfrac{c_{11}+2c_{12}}{3}$, $G=c_{44}$
Young's modulus & Poisson's ratio	$E=\dfrac{9KG}{3K+G}$, $\upsilon=\dfrac{3K\text{-}2G}{2(3K+G)}$
Acoustic Debye temperature[1]	$\theta_D=0.003627\times\left[\dfrac{n\rho}{M(v_s^3+2v_l^3)}\right]^{1/3}v_l v_s$
Acoustic Grüneisen constant	$\gamma=\dfrac{3}{2}\left(\dfrac{3v_l^2-4v_s^2}{v_l^2+2v_s^2}\right)$

1) "M" [kg/mol] represents the Molar mass of materials. "n" is the number of atoms contained in the molecular formula of the material and "ρ" is the density of materials [kg/m^3].

B. Dual-mode ultrasonic timing control method

In order to generate required excitations, acquire data of echoes and analyze acoustic parameters, the ultrasonic measurement system contains three parts: ultrasonic wave generator, FPGA timing system and data acquisition and analysis system. The main structure is shown in Fig.2.

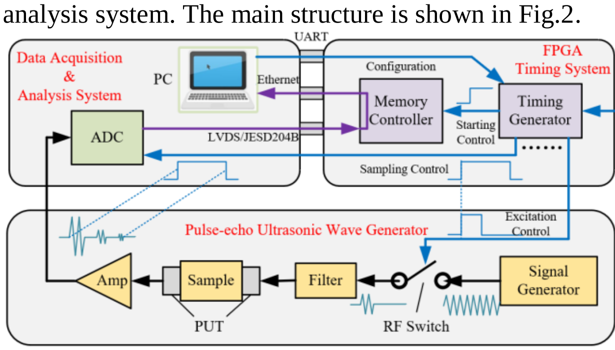

Fig. 2. Main structure of the ultrasonic test system

In the ultrasonic wave generator, a continuous sine wave is generated by the signal generator and chopped by RF switches to be the incident ultrasonic pulse wave, then sent to the sample. The echoes will be acquired by the analog-digital converter (ADC) after amplified and filtered.

The FPGA timing system is the core part of the system, which is the key to meet the four requirements mentioned above. The realization of each function is shown in several parts below:

1) High Resolution and Wide Range for Req.1 & 2

It generates the excitation control timing sequence just at the beginning of the magnetic field to drive the RF switches referring to the external signal. The pulse width of the excitation needs to be in nanosecond level for tiny samples, and the duty ratio should be 10%~20% in the PF-mode and less than 5 ppb in the SF-mode. and the timing sequence needs to be stable for the repetitive measurements and automatic analysis.

To meet these needs, FPGA based two-stage interpolation timing systems are widely used [22],[23] and can be implemented on Xilinx Kintex-7 FPGA to achieve above requirements. The "two-stage" means the "counter + delay chain" cascade structure, which is shown in the Fig.3.

When the external trigger is acquired by the clock of FPGA, an internal reference edge is generated (① in Fig.3) and all the timing channels begin to delay the timing edge to the target position. Referring to the main clock of 200 MHz, a timing resolution of 5 ns can be achieved by the counter as the first stage (② in Fig. 3). It's possible to implement a 32-bit counter in FPGA to generate a single pulse with the width of more than 20 seconds, making it possible to realize a duty ratio of 0.23 ppb. The second stage is the IDELAYE2 delay chain (④ in Fig.3) in Xilinx FPGA to deal with some precise timing adjustment, a single tap of which represents a delay of 78 ps referring to 200 MHz clock.

At the end of one delay action, a new reference is generated and another action is started according to new control data (getting from the Memory Interface Generator (MIG)) including number of counter and IDELAYE2 stages in use. The first stage meets the fundamental requirement of resolution for the excitation control and the wide range of pulse width adjustment. And the second edge make it possible to precisely adjust the sampling window with a resolution of 78 ps.

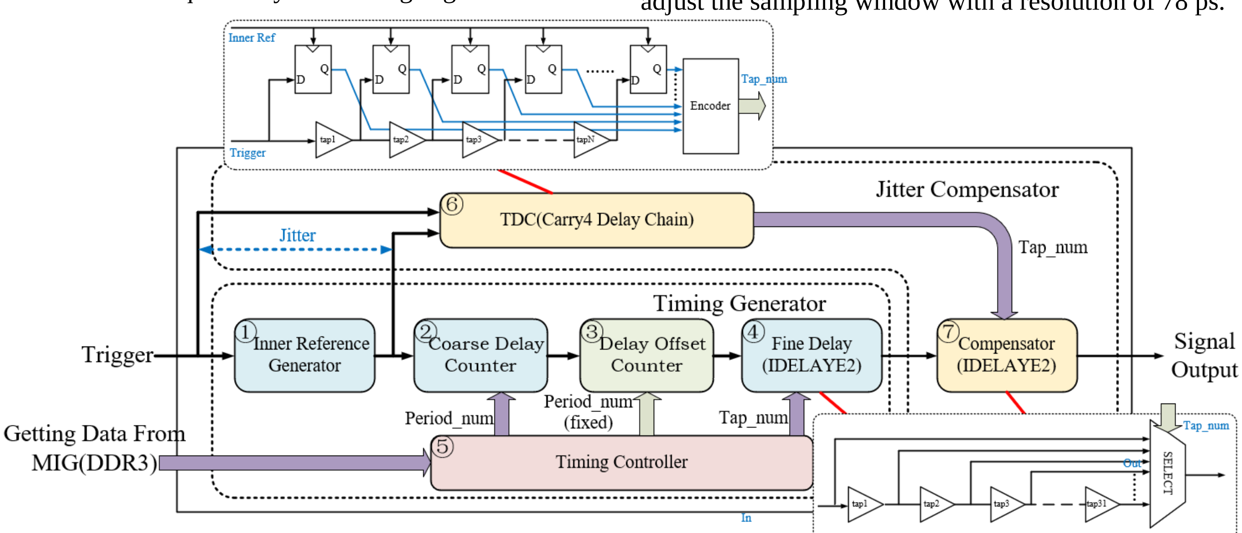

Fig. 3. Structure of the on-chip timing control system in the FPGA

2) Data Size Reduction for Req.3

Meanwhile, another timing sequence channel with a small offset to the excitation (shown in Fig.3) is needed to control and adjust the sampling window, which is used to select the signal section needed freely and accurately, reduce the data size and extend the maximum test duration. This function can be realized by the implementation of multi-channel timing generation and an optional small offset stage (③ in Fig.3) in the timing generator. The Period_num of the attached offset counter is configured after the system powered on and can be adjusted in real-time. This extra stage makes it possible to adjust the sampling window within a wider dynamic range of several microseconds. And it will be acceptable to keep the two channels just synchronous.

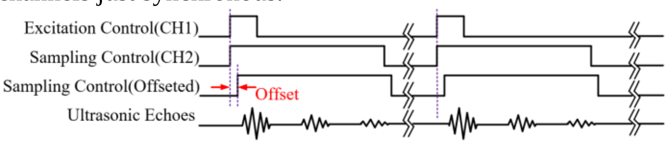

Fig. 4. Timing relationship among the excitation, the sampling window and the ultrasonic echoes

The data size reduction rate can be calculated as:

$$R = 1 - \frac{Sampling\ Window\ Size}{Testing\ Interval} = 1 - \frac{2.5 \sim 3.5 * TOF}{Testing\ Interval} \quad (4)$$

The data compress rate relies on the actual testing interval and the average TOF of sample, and will be ultra-high when deal with the SF-mode tests.

3)Accurate and Stable External Trigger Mode for Req.4

Excitation must be generated just at the beginning of the magnetic field. However, there is always an uncertain jitter between external trigger itself and its acquisition moment, which may induce the actual resolution of timing control [24],[25]. To keep the accuracy of excitation generating control and sampling window adjustment, a "carry-chain based time-digital converter (TDC) + IDELAYE2 based digital-time converter (DTC)" (⑥ and ⑦ in Fig.3) structure [17] is used to timely figure out the jitter size and carry out the compensation. The timing sequence diagram of the complete delay process is shown in Fig.5.

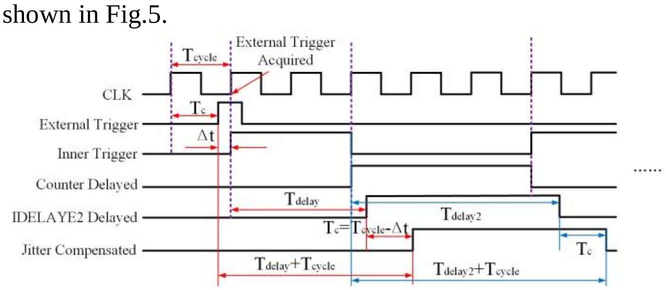

Fig. 5. Timing diagram of the two-stage interpolation delay process (without offset)

Finally, after the system powered on, set up the timing control data on the personal computer (PC) though a universal asynchronous receiver-transmitter (UART) and wait for the external trigger that represent the formation of magnetic field, the excitation of ultrasonic waves and data acquisition will be started automatically. All these processes can be operated on the self-designed LabVIEW software, as well as the automatic cross-correlation and FFT analysis.

III. SET-UP OF EXPERIMENTS

A. Signal Generating System

The structure of the whole ultrasonic measurement system has been shown in Fig.2. A function generator (DSG821 from RIGOL™) is used to provide a continuous sine wave with a certain frequency. The sine wave is chopped by two RF switches (ZYSWA-2-50DR+ from Mini-Circuits™), enhanced by a gain block (ZFL-1000VH+ from Mini-Circuits™) and transmits to the customized 10° Y-rotated $LiNbO_3$ transducer (in the homemade sample probe). The echoes are amplified by a two-stage amplifier (MAR-6+ from Mini-Circuits™) and then sent to the ADC. The structure of the electrical parts and the sample rod is shown in Fig.6:

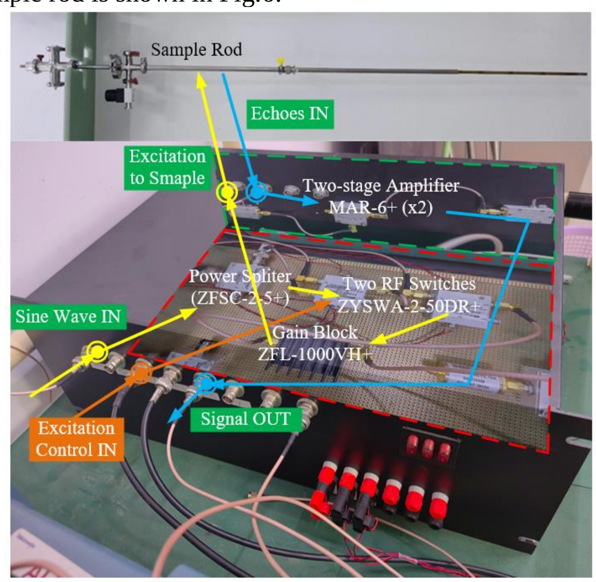

Fig. 6. Structure of the acoustic signal generating circuits and the sample rod used in the high magnetic field tests

B. On-board Controlling System

The implemented structure of on-board system is shown in Fig.7.

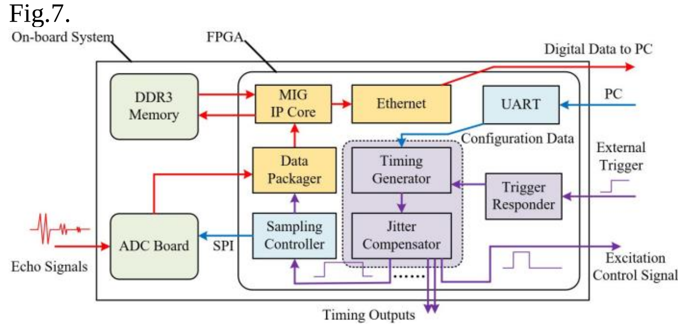

Fig. 7. Main structure of the on-board controlling system

The timing control system is implemented on the Xilinx Kintex-7 FPGA XC7K325T. A 4-channel AD9627 ADC with 125MSps sampling rate and 12-bit resolution is used to acquire the ultrasonic echoes below 40MHz. A 2-channel ADS54J42 ADC with 625 MSps sampling rate and 14-bit resolution can be applied in the future if data sampling of ultrasonic signals from 40MHz to 150 MHz is required. In addition, there are 2 GB double-data-rate-3 (DDR3) memory, an UART port and an ethernet interface in system.

The "counter + IDELAYE2" based two-stage interpolation timing generation module in FPGA has been tested by both simulation and board-level verification. Experiments have been done in our previous research [17] and the results show that the timing generator can reach a resolution of 5 ns by the first stage for the excitation control, and a higher precision of 78 ps by the second stage for the adjustment of the sampling window. And previous long-term tests [17] show that the jitter of this timing system can maintain within 160 ps when the environment changes or the time courses.

In addition, the UART module for timing control data transportation, the serial-peripheral-interface (SPI) module for ADC configuration, the ADC sampling control module, the ethernet data uploading module and the DDR3 memory read-write control module for data used in all modules above are integrated on FPGA and designed with Verilog. The resource occupation of the on-chip system is summarized in Table.II.

TABLE II
RESOURCE OCCUPATION OF THE ON-CHIP SYSTEM IN FPGA

	LUT	Slice	Flip-flop	LUTRAM	BRAM
Utilization	18982	8293	20125	1833	128.5
Available	203800	50950	407600	64000	445
Occupation Rate (%)	9.314	4.937	16.277	2.864	28.876

C. Set-up of Static Field Mode Tests

In the SF-mode tests in stable magnetic field or no field environment, excitation signal is emitted by the signal generator with a frequency of 18 MHz and a -3 dBm power and be sent to the 10° Y-rotated $LiNbO_3$ transducer after two-stage amplifier and filter. The length of the Quartz is 2 cm put outside the magnet, whose standard transverse sound velocity is about 3800m/s. Set the pulse width of the excitation to 1μs and the interval between two tests to 2 seconds (by setting the Period_num with the combination of 200 and 399999800). Meanwhile, let the size of the sample window be 20 μs and have the same repetition rate as the excitation (set with 2000 and 399998000) to realize a data size reduction rate of more than 99%. Finally, when the external trigger comes, the timing generation starts and enable all the functions, making the process of "excitation, sampling, transportation, acoustic analysis" be done automatically in each 2 seconds. The effective part of the excitation signal and the sampling window are shown in Fig.8:

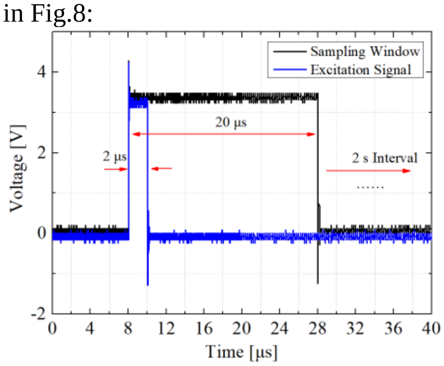

Fig. 8. Timing signals used in the SF-mode tests including the excitation signal (blue) and the sampling window control signal (black)

D. Set-up of Pulsed Field Mode Tests

Based on the high magnetic field of WHMFC, a pulsed magnetic field with a maximum of 55 T and a duration of 160 ms can be generated for our tests. The magnetic induction intensity reaches the peak in 20 ms, and the waveform is shown in Fig.9. Ultrasonic tests in pulsed magnetic field and lower temperature (1.7 K ~ 1.8 K) are carried out to verify the function of the system in the tests in extreme conditions.

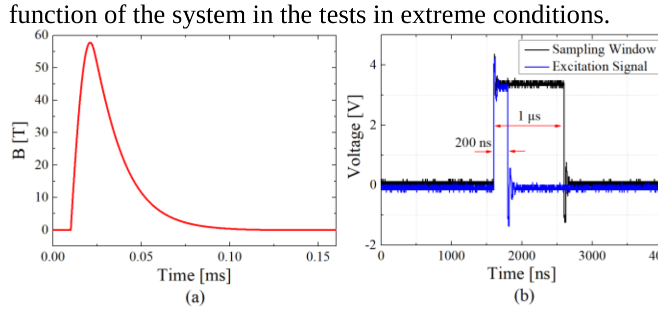

Fig. 9. Waveform of the magnetic field (a) and the Timing signals (b) used in the PF-mode tests

Adjust the excitation frequency to 35.8 MHz which equals to the absorption peak shown in the network analyzer (ZNL3 from Rohde & Schwarz^{TM}), and put the $CeRhIn_5$ sample with the length of 2.38 mm and the transducers (**k**//**u**//[110], where **k** is the ultrasound prorogation vector, **u** is polarization of the ultrasound wave.) into the narrow space inside the magnet and excite it with the same transducer. This configuration provides a measure of $(C_{11}+C_{12}+2C_{44})/4$. Set the excitation width to 200 ns and the repetition rate to 100 kHz. The sampling window has a size of 1 μs and is synchronized with the excitation with a small time offset to realize a data size reduction rate of 90%. The external trigger is generated when the magnetic field grows to 0.1 T. Then, the timing generation starts, and hundreds of thousands of tests are done quickly in the 160 ms duration. Data are acquired and transported to the PC during the tests and be analyzed all together by the software platform after the measurement completed.

IV. RESULTS AND DISCUSSION

A. Static Field Mode Results of Quartz

The pulse-echoes under a single excitation has been shown in Fig.10, given by the oscilloscope (MDO3000 from Tektronix^{TM}). Adjust the position of the sampling window about 1μs later than the excitation to abandon the cross-talk at the beginning. Then, the ultrasonic echoes are acquired by the ADC in the shape of its original waveforms.

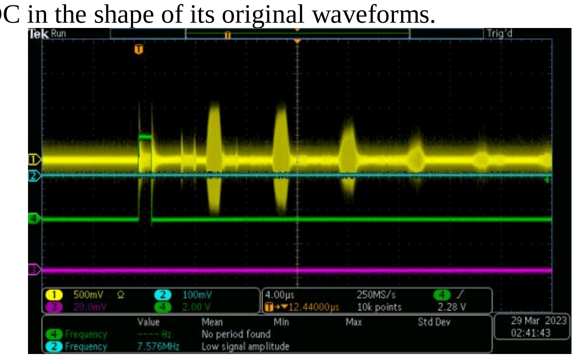

Fig. 10. Single excitation (green) and the corresponding acoustic echoes (yellow) in the SF-mode test for Quartz

Once the end of the sampling window comes, data of all the echoes that belongs to this excitation will be sent to the PC software. The position of each echo can be recognized approximately by the threshold method or artificial observation. If the beginning of the first two echoes are determined, echoes' positions under other excitations can be automatically defined because the interval between excitations is a constant and the timing generation maintains high stability. According to the approximate location, two parts of signal with the length a little bit longer than the pulse width will be chopped. Then, the cross-correlation and FFT will be carried out to obtain the velocity and attenuation. As there is less relevance between the accuracy of the FFT and the timing resolution, only the velocity results will be discussed later in this paper.

To ensure the accuracy of the analysis and verify our ultrasonic control functions, a prearranged experiment and artificial observation are used to adjust the position of the sampling window precisely. After being chopped from the echo sequence, echoes are interpolated by the "Sinc-interpolation" method to reduce the influence of sampling rate on the accuracy of the analysis. And after cross-correlation calculation, Hilbert transformation will be used to get the envelope of the correlation waveform to enhance the resolution of peak search. After tests about 4 hours, the velocity-time curve given by the software is shown in Fig.11.

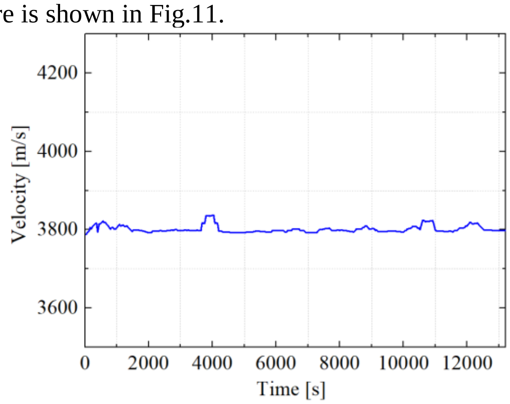

Fig. 11. "Velocity-time" curve for Quartz in the SF-mode tests

It can be seen that the sound velocity of the Quartz keeps between 3800 m/s and 3840 m/s with a very small fluctuation, which is consistent with the theoretical results under normal atmospheric temperature without magnetic field. SF-mode will be the better choice when the sample needs to be monitored in the long term or the researches of the changes of other factors are carried out while the magnetic field keeping unchangeable.

B. Pulsed Field Mode Results of $CeRhIn_5$

One of the echo sequences of the $CeRhIn_5$ is shown in Fig.12, which can be verified to be consistent with the waveform captured by oscilloscope. Considering the rising and falling edge of each echo, the actual pulse width will be about 300 ns. The first three echoes are picked to analyze the velocity and attenuation.

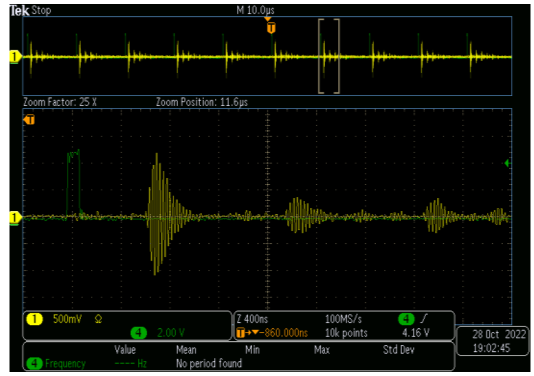

Fig. 12. Acoustic echoes under single excitation in the PF-mode test for $CeRhIn_5$

Different with the SF-mode, this experiment keeps a high repetition rate of excitation during the short duration of 55 T pulsed magnetic field. Only timing generation and data acquisition can be done after each excitation, and the data transportation will be ongoing quickly but much slower than ADC acquisition until all the data in DDR3 are received by PC. The process of data analysis is as same as the SF-mode, after which a velocity-time curve can be calculated. The velocity-time curves in three individual tests at 1.83 K, 1.71 K and 1.70 K are shown in Fig.13:

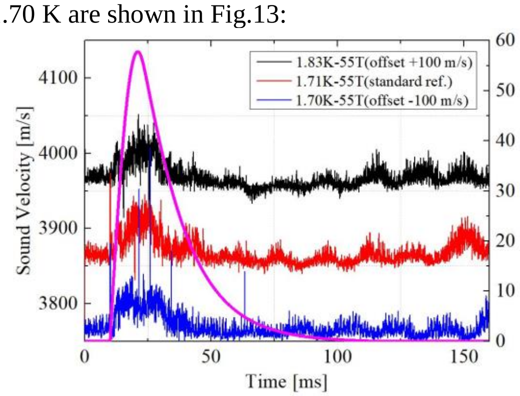

Fig. 13. Sound velocity and 55T background magnetic field curves in the PF-mode tests for $CeRhIn_5$ at 1.7 ~ 1.83 K

Combined with the B-T curve given above, a v-B curve can be plotted and the variety rule of velocity with the change of the magnetic field, as shown in Fig.14.

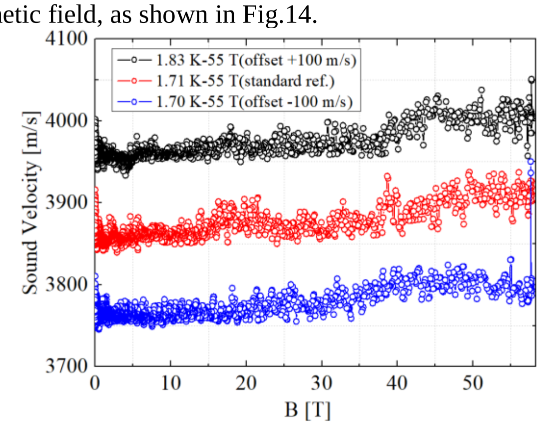

Fig. 14. "Velocity-field intensity" curves in the PF-mode tests at 1.7 ~ 1.83 K

According to the results, the error of the velocity measurement is estimated to be about 40 m/s (about 1%). Compared with the maximum of the velocity changes of about 200 m/s, it can be obviously observed that the ultrasonic velocity apparently changes at the magnetic field point of 42 T, which may be the phase transition point. Owing to the local temperature rise in the sample rod and the changes of C_{11} and C_{44} offset each other, the sound velocity changes little at 20 ~ 30 T. To observe the quantum oscillation phenomena, there are still large number of experiments in pulsed magnetic field to be carried out in higher magnetic field and lower temperature.

V. Conclusion

We propose a "dual-mode" ultrasonic measurement system based on the high-performance timing control implemented on FPGA, aiming at meeting the requirements of ultrasonic experiments in both pulsed and stable magnetic field. For the **Req.1&2**, using the two-stage interpolation delay method, a high resolution of 5 ns/78 ps, wide delay range of 5 ns~21.5 s can be achieved for both precise pulse width control in the PF-mode and large interval in the SF-mode. For the **Req.3**, the multi-channel structure and the configurable offset delay stage make it possible to adjust sampling window control, acquires echoes accurately, compress the data size by more than 80%, and extend the maximum testing duration in both modes. For the **Req.4,** the jitter compensation module for the external trigger realizes a jitter of 160 ps in external trigger mode to maintain the stability of timing control. Combined with the software platform including automatic cross-correlation and FFT analysis and control modules for other interface, a complete dual-mode ultrasonic control and automatic parameter analysis system is implemented with the sound velocity accuracy better than 2%. The system has been preliminarily verified by the ultrasonic experiments of Quartz in SF-mode and $CeRhIn_5$ in the 55 T pulsed magnetic field and low temperature. By improving the thermal retardation capability of the sample rod and increasing the sample rate, this system may be much more helpful to carry out a series of experiments in condensed matter physics or be applied in other industrial measurements.

Acknowledgment

The authors would like to thank Zhenglei Wang, Shaozhe Zhang of WHMFC for the help with this manuscript. This work was supported by the National Key R&D Program of China (2022YFA1602602), the National Key Research and Development Program of China (Grant No. 2016YFA0401703), and the National Natural Science Foundation of China (Grant No. 51821005).

References

[1] Kohama Y, Nomura T, Zherlitsyn S, et al, "Time-resolved measurements in pulsed magnetic fields," *Journal of Applied Physics*, vol.132, no.7, Aug. 2022, Art.no. 070903.

[2] Kurihara R, Miyake A, Tokunaga M, et al, "High-field ultrasonic study of quadrupole ordering and crystal symmetry breaking in $CeRhIn_5$," *Physical Review B*, vol.101, no.15, Apr. 2020, Art.no. 155125.

[3] Mishra S, Gorbunov D, Campbell D J, et al, "Origin of the 30 T transition in $CeRhIn_5$ in tilted magnetic fields," *Physical Review B*, vol.103, no.16, Apr. 2021, Art.no. 165124.

[4] Ramshaw B J, Modic K A, Shekhter A, et al, "Quantum limit transport and destruction of the Weyl nodes in TaAs," *Nature Communications*, vol.9, no.1, Jun. 2018, Art.no. 2217.

[5] Wolf B, Zherlitsyn S, Schmidt S, et al, "Soft acoustic modes in the two-dimensional spin system $SrCu_2(BO_3)_2$," *Physical Review Letters*, vol.86, no.21, pp. 4847-4850, May. 2001.

[6] Zherlitsyn S, Yasin S, Wosnitza J, et al, "Spin-lattice effects in selected antiferromagnetic materials," *Low Temperature Physics*, vol.40, no.2, pp. 123-133, Mar. 2014.

[7] Tsurkan V, Zherlitsyn S, Felea V, et al, "Magnetostructural transitions in a frustrated magnet at high fields," *Physical Review Letters*, vol.106, no.24, Jun. 2011, Art.no. 247202.

[8] Yanagisawa T, Hidaka H, Amitsuka H, et al, "Evidence for the single-site quadrupolar Kondo effect in the dilute non-kramers system $Y_{1-x}Pr_xIr_2Zn_{20}$," *Physical Review Letters*, vol.123, no.6, Aug. 2019, Art.no. 067201.

[9] Tsurkan V, Zherlitsyn S, Yasin S, et al, "Unconventional magnetostructural transition in CoCr 2 O 4 at high magnetic fields." *Physical review letters*, vol.110, no.11, Mar.2013, Art.no. 115502.

[10] Zabbal P, Ribay G, Jumel J, "Evaluation of metallic bonded plates with nonlinear ultrasound and comparison with destructive testing," *NDT & E International*, vol. 123, Oct. 2021, Art.no. 102514.

[11] Ye D, Yin C, Xu Z, et al, "Feasibility of using ultrasonic-based prediction for hydrogen embrittlement susceptibility of high-strength heat-resistant steel 2.25 Cr-1Mo-0.25 V," *Measurement*, vol. 196, Jun. 2022, Art.no. 111162.

[12] S. Wang et al., "Upgrade of the Pulsed Magnetic Field System With Flat-Top at the WHMFC," in IEEE Transactions on Applied Superconductivity, vol. 30, no. 4, pp. 1-4, June 2020, Art no. 4900404, doi: 10.1109/TASC.2020.2969108.

[13] Wolf B, Lüthi B, Schmidt S, et al, "New experimental techniques for pulsed magnetic fields–ESR and ultrasonics," *Physica B: Condensed Matter*, vol.294, pp. 612-617, Jan. 2001.

[14] Suslov A, Sarma B K, Ketterson J B, et al, "Ultrasonic instrumentation for measurements in high magnetic fields. II. Pulsed magnetic fields," *Review of scientific instruments*, vol.77, no.3, Mar. 2006, Art.no. 035105.

[15] Tan C, Li X, Liu H, et al, "An ultrasonic transmission/reflection tomography system for industrial multiphase flow imaging," *IEEE Transactions on Industrial Electronics*, vol.66, no.12, pp. 9539-9548, Dec. 2019.

[16] Haldren H A, Perey D F, Yost W T, et al, "A digital, constant-frequency pulsed phase-locked-loop instrument for real-time, absolute ultrasonic phase measurements," *Review of Scientific Instruments*, vol.89, no.5, May. 2018, Art.no. 054902.

[17] Qiu W, Xie J, Liu Q, et al, "A low-jitter timing generator based on completely on-chip self-measurement and calibration in a field programmable gate array," *Review of Scientific Instruments*, vol.92, no.11, Nov. 2021, Art.no. 114703.

[18] Fang Z, Su R, Hu L, et al, "A simple and easy-implemented time-of-flight determination method for liquid ultrasonic flow meters based on ultrasonic signal onset detection and multiple-zero-crossing technique," *Measurement*, vol.168, Jan. 2021, Art.no. 108398.

[19] Yang Z, Yan W, Li F, et al, "Evaluating onset times of acoustic emission signals using histogram distances," *IEEE Transactions on Industrial Electronics*, vol.68, no.6, pp. 5237-5247, Jun. 2021.

[20] Jia L, Xue B, Chen S, et al, "A high-resolution ultrasonic ranging system using laser sensing and a cross-correlation method," *Applied Sciences*, vol.9, no.7, Apr. 2019, Art.no. 1483.

[21] S. Sun, S. Li, L. Lin, Y. Yuan and M. Li, "A Novel Signal Processing Method Based on Cross-correlation and Interpolation for ToF Measurement," 2019 IEEE 4th International Conference on Signal and Image Processing (ICSIP), Wuxi, China, 2019, pp. 664-668.

[22] Qin X, Zhang W Z, Wang L, et al, "A pico-second resolution arbitrary timing generator based on time folding and time interpolating," *Review of Scientific Instruments*, vol.89, no.7, Jul.2018, Art.no. 074701.

[23] Zhang W Z, Qin X, Wang L, et al, "A fully-adjustable picosecond resolution arbitrary timing generator based on multi-stage time interpolation," *Review of Scientific Instruments*, vol.90, no.11, Nov. 2019, Art.no. 114702.

[24] Chen Z, Wang X, Zhou Z, et al, "A simple Field Programmable Gate Array (FPGA) based high precision low-jitter delay generator," *Review of Scientific Instruments*, vol.92, no.2, Feb. 2021, Art.no. 024701.

[25] J. Li, Z. Zheng, M. Liu and S. Wu, "Large Dynamic Range Accurate Digitally Programmable Delay Line with 250-ps Resolution," 2006 8th international Conference on Signal Processing, Guilin, China, 2006, pp. , doi: 10.1109/ICOSP.2006.345484.